infrastructures

MDPI

Review

Numerical Modeling of Cross-Laminated Timber (CLT) Shear Wall Structures: Review and Assessment

Tian Xia, Yuntian Wu * and Ahmed Ibrahim

Department of Civil and Environmental Engineering, University of Idaho, Moscow, ID 83844, USA; xia1762@vandals.uidaho.edu (T.X.); aibrahim@uidaho.edu (A.I.)
* Correspondence: yuntianw@uidaho.edu

Abstract

Recent revisions to the International Building Code (IBC 2021) have allowed high-rise mass timber shear wall structures up to 18 stories and 270 feet, reflecting the growing popularity and wide recognition of the advantages of mass timber construction. However, research on high-rise mass timber lateral force resisting systems (LFRSs) has heavily relied on experimental studies. Numerical modeling techniques for mass timber shear walls remain limited in terms of generality and applicability, which significantly hinders the further development of design and analysis methods for high-rise mass timber structures in medium-to-high seismic regions. In this paper, the strategies and characteristics of different numerical models of cross-laminated timber (CLT) shear walls are systematically reviewed and discussed. To assess the applicability of different models, a basic panelized CLT shear wall is selected as a benchmark for evaluating and comparing different modeling approaches in terms of their global hysteretic response, deformation characteristics, and computational efficiency. Recommendations are provided for the selection of numerical modeling approaches for various design and analysis scenarios. Future research needs in the nonlinear numerical simulation of CLT shear wall structures are identified and discussed.

Keywords: mass timber; CLT; numerical model; lateral force resisting system; shear wall

1. Introduction

The 2021 International Building Code (IBC) introduced a significant revision that allows high-rise mass timber shear wall buildings up to 18 stories and 270 feet (Type IV-A) [1]. This revision reflects the recognition of the sustainability, constructability, and overall economy of mass timber construction as an alternative to traditional steel and concrete constructions [2,3]. Among different mass timber materials (e.g., glulam and laminated veneer lumber), cross-laminated timber (CLT) is highly suitable for use in shear walls because of its significant strength and stiffness when subjected to in-plane forces [4]. However, current adoption of CLT in high-rise buildings is mainly for the gravity system only. The CLT lateral (seismic and wind) force resisting system (LFRS) is rarely used in high-rise structures due to code restrictions and insufficient research. Panelized CLT shear walls, the only codified CLT LFRS for multi-story buildings, utilize small and interconnected CLT panels to provide adequate deformation capacity and energy dissipation under seismic loading. However, this structural configuration largely reduces the lateral stiffness as the structural height increases, leading to a structural height limit of 65 ft in mid-to-high seismic regions [5]. Therefore, the vast majority of high-rise mass timber buildings

Check for updates

Academic Editor: Mi G. Chorzepa

Received: 4 September 2026
Revised: 5 October 2026
Accepted: 5 October 2026
Published: 8 October 2026

Copyright: © 2026 by the authors. Licensee MDPI, Basel, Switzerland. This article is an open access article distributed under the terms and conditions of the Creative Commons Attribution (CC BY) license.

use hybrid systems, combining the mass timber gravity system and steel or concrete lateral system [6].

Driven by the benefits of all-timber construction, research on high-rise CLT shear wall structures using the FEMA P-695 validation process [7] has been ongoing in the U.S. Based on the development of concrete and steel rocking systems, CLT rocking shear walls were developed for use in high-rise mass timber buildings in high seismic regions. Deviating from panelized CLT walls, CLT rocking systems facilitate controlled deformation and energy dissipation through their ability to rock and lift at one end during seismic events, often involving the use of post-tensioning (PT) hold-downs and supplemental energy dissipation devices [8]. Other proposed high-rise CLT LFRSs include post-tensioned C-shaped CLT shear walls [9], hybrid coupled CLT shear walls with steel link beams [10], and pivoting walls with buckling-restrained boundary elements [11]. However, current research on mass timber high-rise LFRSs remains dominated by experimental investigations, with numerical simulation serving as a supplementary tool only. Each numerical model has to be calibrated using the corresponding experimental results and cannot be used for a simulation involving different details from the experimental model for calibration. This differs markedly from the research approaches commonly adopted for steel and concrete structures. In the seismic design and analysis of steel and concrete structures, the philosophy of "strong connections and weak members" is followed such that nonlinear behavior is concentrated in selected structural members such as beams and bracing elements. In addition, the constitutive relationships and failure criteria for steel and concrete materials are well established. Numerical modeling can effectively capture the nonlinear responses and failure process of these structures. By contrast, the nonlinear response usually develops and concentrates at the connections of mass timber LFRSs. For example, at the failure of CLT shear walls, the wall panels generally remain elastic, while the hold-downs and angle brackets suffer from significant deformation and damage. Therefore, for mass timber LFRSs, the key challenge in numerical simulation is not only the consideration of the constitutive behaviors and failure criteria of engineered wood products (e.g., mass timber) that are more complicated than those of conventional homogeneous materials, but also the appropriate characterization of the force transfer, deformation, and failure mechanisms of the connectors. However, the connections used in mass timber systems are highly diverse, and their mechanical behaviors are influenced by a number of factors, including connector material and type, connection detailing, and timber–connector interaction. To further investigate mass timber high-rise lateral force resisting systems, numerical models for thorough parametric studies, performance assessment, and full-scale structural analyses are urgently needed.

Although a wide range of numerical modeling approaches has been developed for CLT shear wall structures over the past two decades, these models are specifically developed and tailored for their specific experimental studies. Little effort has been devoted to comprehensive comparison and assessment of these models, leaving their capabilities, limitations, and appropriate application scenarios insufficiently understood. To address this gap, this paper comprehensively reviews the numerical modeling strategies used for the simulations of the key mechanical behaviors of CLT shear wall structures. Existing numerical models are first classified according to their degree of idealization and element selection. The modeling characteristics of each category are discussed. A panelized CLT shear wall is then adopted as a benchmark case to assess and compare representative modeling approaches. Finally, future research needs in the nonlinear numerical simulation of CLT shear wall structures are discussed.

2. Modeling Strategies

Adequate simulation of the structural response of CLT shear wall structures largely depends on the proper modeling of (1) the mechanical behavior of wall panels; (2) the contact behavior between panels; (3) the connection behavior; and (4) the self-centering behavior. This section systematically reviews the modeling approaches for these fundamental behaviors, thereby establishing the basis for the subsequent classification and assessment.

2.1. CLT Wall Panel Modeling

2.1.1. Material Model

Extensive experimental investigations on CLT shear walls have shown that the wall panels remain largely elastic throughout the loading process [12]. Instead, nonlinear responses are primarily concentrated at the wall-to-base connections and in the wall corner regions. Consequently, CLT panels are commonly modeled as elastic components. To account for the orthogonal layup of CLT laminations, several studies have employed orthotropic material models to represent the behavior of CLT panels [13–16]. Alternatively, other researchers have adopted isotropic elastic material models, in which equivalent elastic and shear moduli are used to characterize the overall mechanical behavior of the panels [17–22]. Hummel et al. [17] reported that the global response of CLT shear walls is not significantly affected by the use of isotropic versus orthotropic material properties. This limited difference can be attributed to the connection-dominated hysteretic behavior of CLT shear walls. Because bending and shear deformations of the CLT panels contribute only a small portion of the total lateral displacement [12], the choice of elastic material formulation has a limited influence on the global hysteretic response. Similarly, the mesh size of the CLT panels generally has a limited influence on the global structural response. Therefore, isotropic elastic material models and reasonably selected meshes can be sufficient for capturing the global structural behavior of CLT shear walls while offering a simpler and more computationally efficient modeling process.

Although elastic material models are widely adopted in numerical studies, a limited number of researchers have incorporated nonlinear material behavior into CLT panel models. More detailed representations of fiber orientation and material nonlinearity are important when local stresses, deformations, or failure mechanisms are of interest. Wilson et al. [23] assigned different material properties to various regions of the wall panels. An elastic–perfectly plastic constitutive model was used in localized compression zones to simulate crushing behavior, while the remaining regions were modeled as elastic. Akbas [24] and Wang [25] subdivided the wall panel into two regions and modeled the area near the wall base using fiber-section beam elements calibrated to the nonlinear compressive behavior of CLT. This approach enables the localized nonlinear response at the wall base to be explicitly captured.

2.1.2. Element Selection

The numerical modeling of CLT wall panels is commonly based on three categories of elements: solid elements, shell elements, and beam elements. The modeling characteristics, strengths, limitations, and appropriate applications of these element types are discussed in detail in Section 2.

2.2. Contact Behavior

2.2.1. Normal Contact

Normal contact behavior primarily governs the rocking response of CLT shear walls and is a key factor influencing the overall deformation mode of the structure. Under lateral loading, the wall panel rotates, resulting in compression at one edge of the wall–foundation

interface while a gap develops at the opposite edge. Therefore, numerical models should be able to realistically capture the closure, opening, and re-contact process occurring along the contact interface.

The modeling of normal contact behavior generally involves two key considerations. The first is the selection of an appropriate contact modeling approach for adjacent components. The second relates to the definition of contact stiffness, which directly affects the stress distribution within the contact region and the overall structural response. The appropriate stiffness value depends primarily on the material of the contact interface (e.g., CLT-to-CLT or CLT-to-concrete interfaces) and the mechanical properties of the CLT panel [17].

Existing studies have generally adopted three approaches to model normal contact behavior, as shown in Figure 1: (a) Direct definition of contact pairs and contact properties. In this approach, contact algorithms automatically govern contact, separation, and re-contact between adjacent components. Izzi et al. [13] employed hard contact to model the normal interaction between wall panels and the foundation or adjacent panels. To account for interface irregularities associated with construction tolerances, Chen et al. [26] adopted a soft contact formulation, with the contact stiffness between the wall panel and the bottom rigid beam defined as 1% of the longitudinal stiffness of the CLT panel. (b) Rigid wall-to-base connection with incorporation of nonlinear material behavior within a fiber section at the wall base. Unlike contact-based approaches, the rocking behavior is captured implicitly through the sectional response of the fiber element [22–25,27], allowing for the formation of compression zones and a gap opening at the wall base without explicitly modeling the contact interface. (c) Compression-only springs between interface nodes. This is a common approach in both shell element and beam element models. However, the required spring stiffness depends on how compressive deformation is represented. In shell element models, the wall panel is discretized using shell elements, allowing the compressive deformation of the CLT panel to develop directly within the wall. Consequently, the interface springs are usually assigned a large compressive stiffness and function mainly as contact constraints [17,28]. In beam element models, the wall is represented by line elements and cannot explicitly capture local compression at the rocking interface. Therefore, the compressive deformation is concentrated in a multi-spring element placed at the wall base, with spring stiffness K_m calibrated from the compressive properties of the CLT. There are two approaches for stiffness calibration [23]. The first relies on experimental data through transforming the measured stress–strain relationship into an equivalent force–displacement relationship [29]. The second derives the force–displacement relationship directly from the Young's modulus E of CLT [30], as expressed in Equation (1). Determination of the plastic hinge length l_p is of particular importance when using these two approaches. Akbas et al. [24] showed that a plastic hinge length equal to twice the wall thickness b_w can reasonably reproduce the localized compression behavior at the wall base.

For approaches (b) and (c), the compression-only behavior at the wall base is usually represented using constitutive models such as the elastic–no-tension (ENT) material model [31], the elastic–perfectly plastic (EPP) gap material model [24], and the compression-only concrete01 material available in OpenSeesPy platform [32]. The selection of a specific constitutive model generally depends on the availability of experimental data and the required level of accuracy.

$$K_m = \frac{b_w l_w E}{l_p} \tag{1}$$

where l_w is the length of the CLT wall panel.

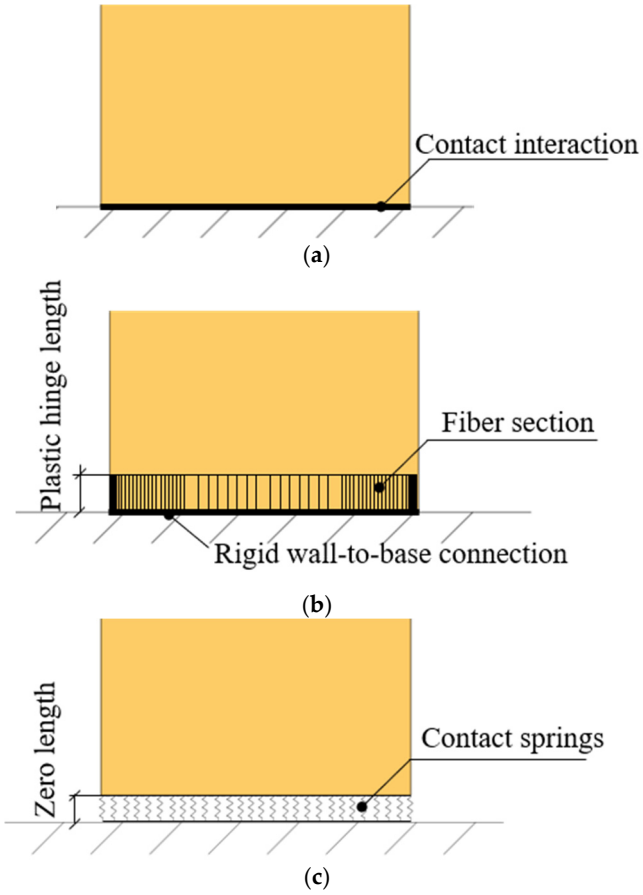


Figure 1. Three approaches for modeling normal contact behavior: (**a**) contact pairs with defined contact properties; (**b**) fiber section with compression-only material; (**c**) compression-only springs.

2.2.2. Frictional Behavior

Frictional behavior is primarily associated with the sliding response of CLT shear walls. The frictional resistance developed at the wall base depends on the normal contact force and varies due to the sliding and rocking behavior of the wall. For numerical robustness, finite element models commonly assume identical static and kinetic friction coefficients. Existing studies have considered tangential friction behavior using the following approaches: (1) Direct definition of tangential contact behavior. Izzi et al. [13] and Chen et al. [26] both incorporated frictional effects through contact algorithms by specifying friction coefficients at the contact interface. (2) Adoption of an equivalent horizontal spring. In some simplified models, frictional effects are implicitly considered by the lateral resistance of horizontal connection elements [33]. However, such approaches are generally unable to capture the coupling between frictional behavior and wall rocking. More refined modeling strategies define frictional resistance as a function of the normal contact force. Hristovski et al. [28,34] developed a friction model using rigid plastic springs based on the Mohr–Coulomb criterion. Chen [35] employed ZeroLengthContact3D elements to account for the coupling between normal and frictional forces. In addition, Hummel [17] combined compression-only normal springs with SingleFPBearing elements and simulated frictional behavior through the definition of an evolving friction coefficient.

2.3. Connection Behavior

2.3.1. Characteristics of Connections Using Different Connectors

The nonlinearity and energy dissipation capacity of CLT shear walls are primarily developed at connections. According to the load transfer mechanism and structural config-

urations, CLT connections can be generally classified into dowel-type and dissipative-type connections. Explicit connection modeling using detailed solid elements often leads to excessive computational cost and convergence difficulties. It is more common to employ nonlinear springs that are calibrated against experimental data to provide equivalent representations of the macroscopic mechanical behaviors of CLT connections.

1. Dowel-type connections

Owing to the relatively low embedment stiffness of wood perpendicular to the grain, dowel-type connections tend to exhibit pronounced slip under cyclic loading. As a result, their hysteretic responses are typically characterized by a distinctive pinching effect, as shown by shape 2 and shape 3 in Figure 2 [14]. To simulate such behavior, various constitutive models have been developed and implemented in different numerical platforms. In ABAQUS, hysteretic behavior can be modeled through user-defined element (UEL) subroutines [13,19,33,36]. In SAP2000, the Pivot model has been adopted to capture stiffness degradation characteristics [23,37]. In OpenSees, dowel-type connections are commonly modeled using zero-length elements combined with constitutive models such as Pinching4 [16,38–40], SAWS [17,41], and DowelType [25,42]. The accuracy of these macroscopic models relies heavily on parameter calibration against experimental results.

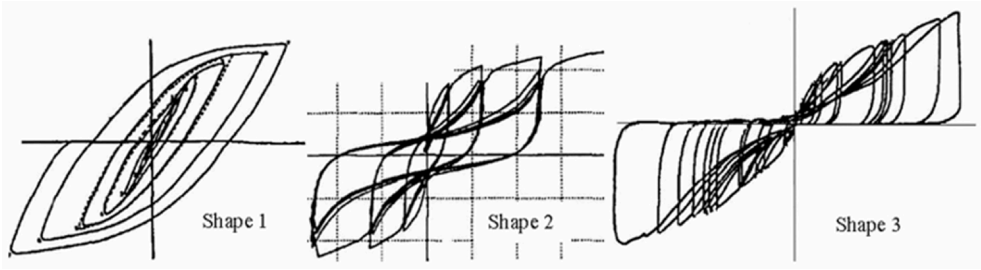


Figure 2. Typical hysteresis shapes for wooden connections [14].

It is worth noting that dowel-type connections, such as steel angle brackets at the CLT wall base, are frequently subjected to combined tension–shear loading. However, most existing constitutive models have been developed and calibrated based on uniaxial tests under either pure tension or pure shear, making it difficult to directly capture tension–shear interaction effects. To address this issue, several numerical studies on CLT shear walls have made assumptions for simplification, such as neglecting the shear resistance of hold-down connections or neglecting the uplift resistance of shear connections [43–45]. However, some researchers [13,46] have argued that the uplift stiffness and shear resistance can significantly influence the lateral performance of CLT shear walls and should not be neglected. To capture this interaction effect, several numerical strategies have been proposed, including the application of strength interaction criteria [33], reduction in connection capacities [17], and the use of coupled elements capable of representing multidirectional responses [15].

2. Dissipative-type connections

Significant pinching and slip limit the hysteretic energy dissipation of traditional dowel-type connections. Various energy-dissipating devices, including X-brackets [47], U-shaped flexural plates (UFPs) [48], O-shaped devices [49], and different dampers [50], have therefore been developed for CLT shear wall connections. These connecting devices mainly rely on the plastic yielding of their core metallic components to dissipate seismic energy. In numerical models such as the Steel02 model in OpenSeesPy [24,51], such metallic components are commonly characterized by elasto-plastic constitutive models capable of capturing cyclic hardening and the Bauschinger effect.

2.3.2. Characteristics of Connections at Different Locations

The influence of a connection on the global structural behavior largely depends on the interaction among the connector and the structural components that it joins. Therefore, increasing attention has recently been devoted to the understanding of connection behavior within the entire structural assembly rather than isolated components. The common connection configurations used in panelized CLT shear wall structures are shown in Figure 3.

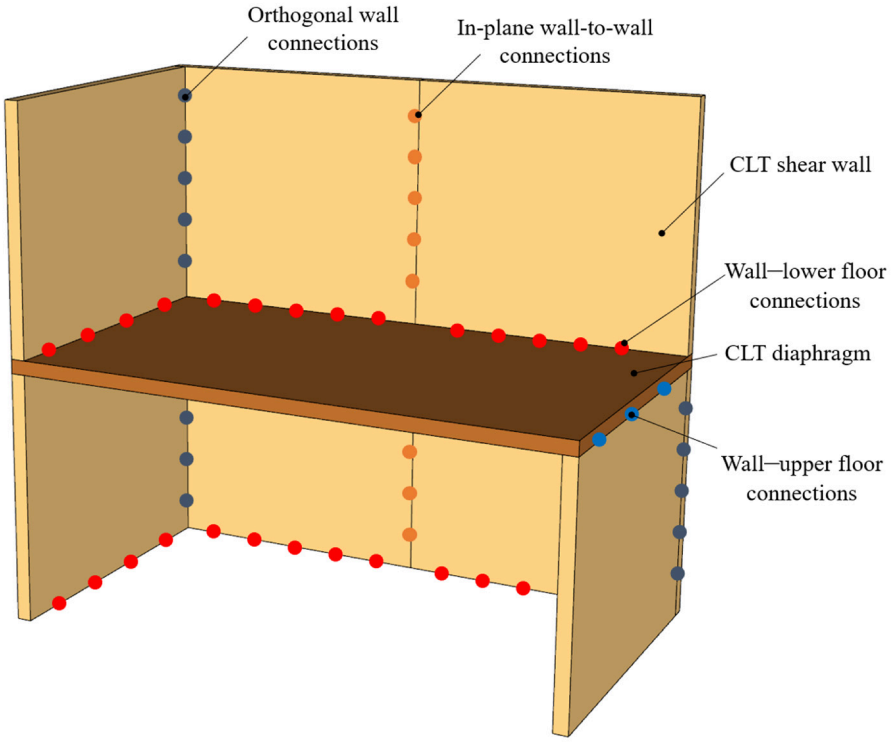


Figure 3. Connections in a CLT shear wall building [52].

1. Wall–lower floor connections

Wall–lower floor connections are commonly achieved through typical dowel-type connections. In numerical models, their behavior is typically modeled using the nonlinear dowel-type hysteretic spring models described in Section 2.3.1. Springs are assigned to the corresponding connection locations to capture the normal and shear resistance of the connectors. The spring properties in the uplift and shear directions are generally calibrated from connection tests, while the compressive response is usually simplified as a linear elastic spring with sufficiently large stiffness [17,33].

2. In-plane wall-to-wall connections

CLT shear walls are commonly assembled from multiple CLT panels connected through vertical joints, such as screwed spline joints, cover-plate connections, or dissipative connectors. Different joint configurations may result in distinct deformation mechanisms [49], as illustrated in Figure 4. In numerical models, these joints are typically modeled using nonlinear hysteretic springs placed along the panel interfaces [24,26,32], with the constitutive model selected according to the connection type. When CLT walls are modeled using beam elements, rigid link elements are commonly introduced between the wall elements and the connection nodes to ensure proper geometric compatibility and deformation continuity [24].

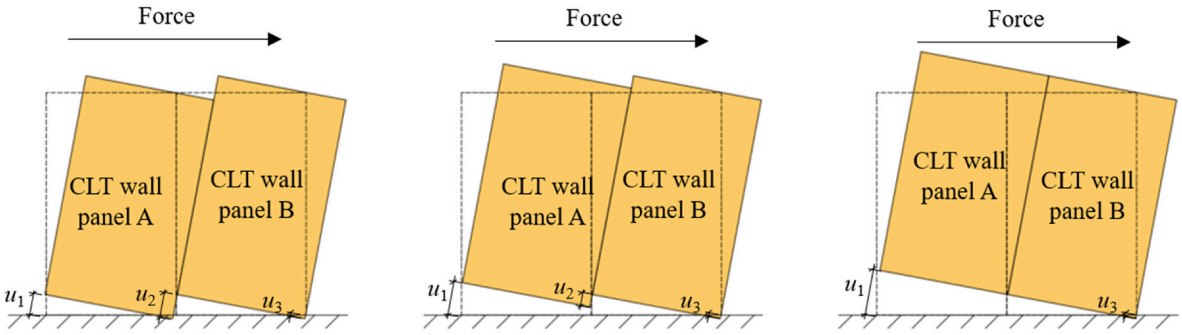


Figure 4. Different deformation modes for walls with in-plane connections [49].

3. Orthogonal wall connections

The presence of orthogonal walls can significantly alter the load transfer mechanism and lateral deformation mode of the primary shear wall. Acting as flange elements, orthogonal walls provide beneficial three-dimensional interaction and can substantially increase the lateral stiffness of the wall assembly. Existing numerical approaches can be broadly categorized into equivalent restraint models and explicit wall models. Equivalent restraint models simplify the effects of orthogonal walls by introducing rigid elements or equivalent boundary conditions [53]. While this approach is computationally efficient, it cannot explicitly capture the deformation and nonlinear behavior of the orthogonal walls or the interaction between intersecting panels. Explicit wall models, in contrast, represent orthogonal walls using structural elements and simulate the interaction between wall panels through nonlinear connection models [53,54]. This approach provides a more realistic representation of three-dimensional wall interactions but at the expense of increased model complexity and computational cost. More importantly, its accuracy depends strongly on the representation of the wall-to-wall connections, which govern force transfer between orthogonal panels.

4. Wall–upper floor connections

Multi-story CLT shear wall structures can generally be classified into balloon-type and platform-type configurations. In balloon-type systems, the influence of floor diaphragms on wall behavior is often limited and can be neglected in numerical models. In contrast, the presence of the floor modifies the load transfer mechanism and deformation characteristics of the wall assembly in platform-type systems. Consequently, numerical models should account for floor-induced effects, including local compression perpendicular to the grain and the contribution of diaphragm stiffness to load transfer between adjacent wall segments. Existing approaches generally represent wall–floor interactions using either detailed contact formulations or simplified spring-based models. Detailed contact formulations can explicitly capture the local interaction and contact-induced deformation at the wall–floor interface, but they may substantially increase model complexity and computational demand, particularly in large-scale dynamic analyses. To reduce this computational burden, simplified approaches replace the distributed interface behavior with equivalent springs or other reduced-order representations [55]. Such simplifications improve computational efficiency, but their ability to reproduce local contact behavior and the resulting force transfer mechanism depends on the adopted spring properties and assumptions.

2.4. Self-Centering Behavior

2.4.1. Effect of Post-Tensioning Tendons

1. PT tendon modeling

PT tendons are commonly modeled using beam [24,31,56], truss [9,32,57,58], or two-node link elements [59,60], depending on the required level of modeling fidelity. Truss elements are the most frequently adopted due to their ability to efficiently capture axial behavior, whereas beam and link elements are typically used when additional geometric or interaction effects need to be considered. The upper end of the tendon is typically connected to the top of the CLT wall through rigid link elements, and the lower end is anchored to the foundation. In simplified macro-models, equivalent rotational springs calibrated against experimental results can also be employed to represent the overall self-centering behavior of the rocking wall structure [32].

2. Prestress application methods

The accurate introduction of prestressing force is critical to PT tendon modeling. Existing studies have generally adopted three approaches to simulate the prestressing process: (a) assigning an initial stress or strain to the tendon material; (b) imposing an initial displacement at the tendon anchorage, and (c) introducing an equivalent thermal strain. The first approach directly establishes the desired prestressing state through material initialization and has been implemented using initial strain formulations [46,59] or the InitStressMaterial in OpenSees [61]. The second approach generates prestressing force through enforced displacement at one end of the tendon [23]. The third approach, commonly adopted in ABAQUS, induces tendon contraction by prescribing a thermal expansion coefficient and applying a temperature reduction to the tendon elements [26].

3. Prestress loss modeling

Prestress loss is primarily associated with residual plastic deformation of the tendons under severe cyclic loading, which may result in the formation of gaps between the anchorage nuts and bearing plates. Accurately representing this mechanism is important for capturing the reduction in tendon force and the associated changes in wall rocking behavior during cyclic loading. Existing numerical approaches generally represent prestress loss either by explicitly modeling the opening and closure of anchorage gaps or by indirectly reproducing the effect through inelastic deformation. Akbas et al. [24] introduced compression-only zero-length contact elements between the tendon anchorage node and the foundation to explicitly capture the opening and closure of anchorage gaps. This approach provides a direct representation of the contact mechanism but requires additional contact elements and may increase model complexity. Alternatively, Sun et al. [31] employed zero-length elements with bilinear elastoplastic constitutive behavior between the tendon anchorage and the foundation, using the accumulated residual plastic deformation of the element to indirectly represent prestress relaxation and loss. Although this approach provides a simpler representation of prestress loss, it does not explicitly reproduce the physical gap-opening and contact mechanism.

2.4.2. Gravity Effects and Geometric Nonlinearity

In addition to post-tensioning tendons, self-centering capability can also be provided by gravity-induced restoring moments. Although the self-weight of an individual wall panel generally contributes only a limited restoring force, the combined gravity loads from floor diaphragms and superimposed dead loads may provide a significant restoring effect at the structural system level. However, large lateral displacements may activate destabilizing P-Δ effects, which reduce the effective restoring capacity and compromise structural stability. Existing numerical models generally account for P-Δ effects using

either direct geometric nonlinear formulations or leaning-column approaches. The former incorporates geometric stiffness through PDelta or Corotational transformations in beam–column elements, whereas the latter employs a leaning column connected to the primary structural system through multi-point constraints to capture P-Δ effects [20–22,27].

3. Classification

This section presents a classification of typical numerical models developed for the two fundamental forms of CLT shear walls, with particular emphasis on nonlinear models. Based on the level of modeling fidelity and the selection of structural components, existing numerical models can be categorized into three groups: high-fidelity model (HFM), component-based model (CBM), and lumped-spring model (LSM). CBM is currently the most widely adopted category and can be further divided into shell element-based and beam element-based models. Beam element-based models mainly consist of fiber-based and multi-spring models. Typical models for panelized CLT shear walls and PT CLT rocking walls are summarized in Tables 1 and 2, respectively, where "△" indicates the capability to represent the mechanism in some models only; "✓" and "✗" indicate the capability and incapability to represent the corresponding mechanism in all models; and "S" and "D" denote static and dynamic time-history analyses, respectively.

Table 1. Typical model of panelized CLT shear wall.

Category	Model	CLT Panel	Contact Behavior		Connection Behavior		Analysis	Description
			Normal	Friction	Connector	Shear–Axial Interaction		
CBM	Shell element-based models [7,17,18,28,31,33,35,36,62–64]	Shell elements	Compression-only springs	△	✓	△	S/D	HA LE
	Fiber-based model [25]	Beam–column elements with fiber section	Fiber section with compression-only material	✗	✓	✗	S/D	MA ME
LSM	Translational spring model [38]	"twoNodeLink element" for lateral performance of wall; "truss element" for compressive stiffness of wall					D	LA HE
	Diagonal spring model [65]	Stiff elastic truss elements at the perimeter; nonlinear springs adopting the hysteresis model of Elwood as diagonals					D	LA HE

The modeling strategies for key mechanisms vary considerably among these model categories, particularly with respect to the normal contact behavior. As shown in Tables 1 and 2, as the level of model simplification increases, fewer mechanisms and interaction effects can be explicitly incorporated into the numerical model. VHA, HA, MA, and LA denote very high, high, moderate, and low modeling accuracy, respectively, while VHE, HE, ME, and LE denote very high, high, moderate, and low computational efficiency, respectively. The qualitative ratings of modeling accuracy and computational efficiency are based on the reported modeling characteristics and computational requirements in the reviewed literature. These ratings are intended to provide a general indication of model applicability rather than quantitative performance scores. The accuracy of each approach depends on the target response, structural configuration, and modeling objectives. This section systematically reviews the fundamental models underlying each category and discusses their advantages, limitations, and suitable applications.

Table 2. Typical models of post-tensioned CLT rocking wall.

Category	Model	CLT Panel	Contact Behavior		Dissipative Connection Behavior	Self-Centering Behavior	Analysis	Description
			Normal	Friction				
HFM	High-fidelity model [26]	Shell element	Softened contact	✓	✓	✓	S	VHA VLE
CBM	Shell element-based models [12,23,56,59,60,66]	Shell element	Compression-only springs	△	✓	✓	S	HA LE
	Fiber-based models [24,27]	Beam–column element with fiber section	Fiber section with compression-only material	✗	✓	✓	S/D	MA ME
	Multi-spring models [32,57,58]	Beam–column element	Compression-only springs	✗	✓	✓	S/D	MA ME
LSM	Rotational spring models [23,32]	Beam–column element	Two rotational springs				D	LA HE

3.1. High-Fidelity Models (HFMs)

HFMs explicitly model structural geometry, material nonlinearities, and contact interactions, enabling accurate simulation of both local and global structural responses. Three-dimensional solid and shell elements are most commonly employed to model the CLT panels. The numerical models in this category can directly simulate complex failure mechanisms, including wood crushing, embedment deformation, and connection yielding, with minimal reliance on experimental calibration. For example, Chen et al. [26] developed a high-fidelity ABAQUS model of a PT CLT rocking wall (Figure 5), in which localized failure mechanisms were successfully captured using only geometric and constitutive information as input parameters.

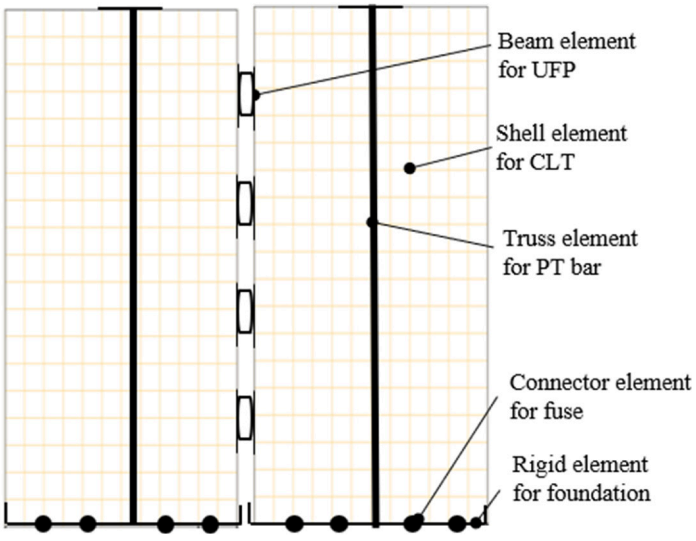


Figure 5. Typical high-fidelity model [26].

Despite their superior accuracy, the application of HFMs remains limited by their high computational cost and convergence challenge. Consequently, HFMs are primarily applied to static or quasi-static analyses of individual shear walls and local connections [67], while their use in nonlinear dynamic analyses of multi-story structural systems remains relatively rare.

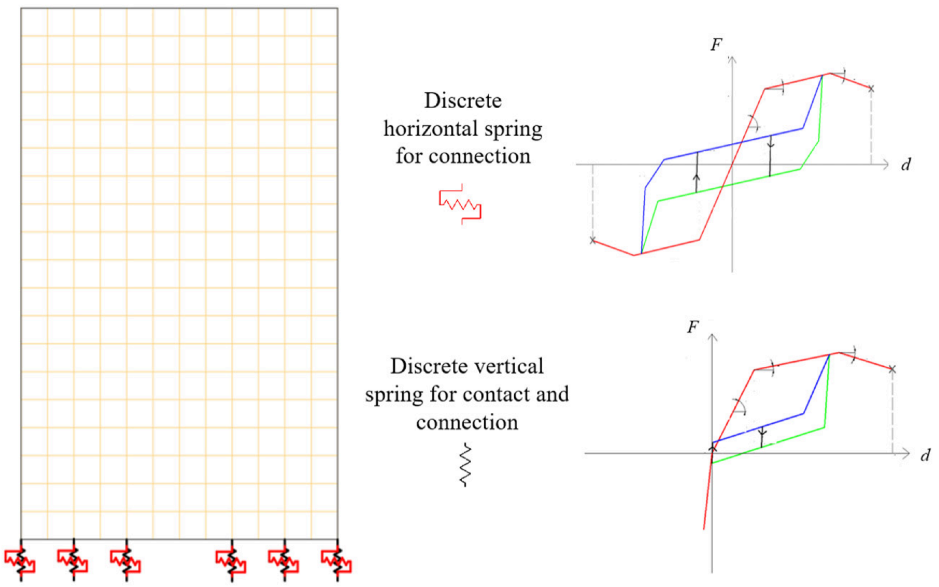
3.2. Component-Based Models (CBMs)

The fundamental concept of CBMs is to explicitly model the primary structural components while simplifying connection behavior through equivalent constitutive relationships. Details regarding connection types, constitutive models, and approaches for capturing the tension–shear interaction are presented in Section 2.3.1.

3.2.1. Shell Element-Based Models

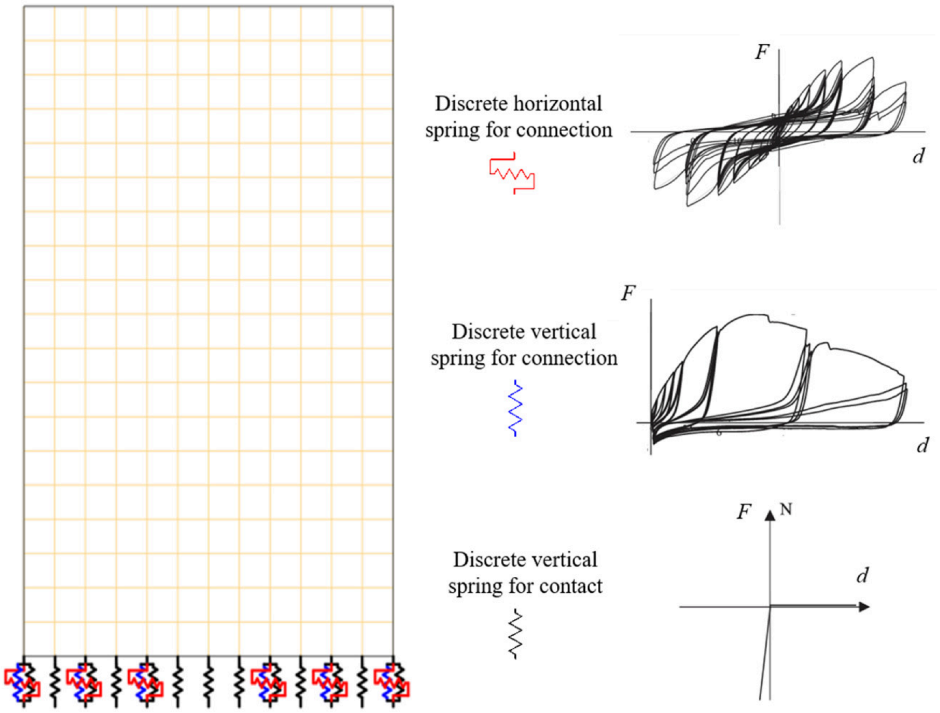
Shell elements are the most widely used element types for modeling CLT wall panels. Compared with three-dimensional solid elements, shell elements do not explicitly resolve through-thickness stresses and deformations, resulting in a substantially lowered computational cost and an acceptable dominant in-plane behavior simulation of CLT wall panels. However, the through-thickness simplification inherent in shell elements introduces certain limitations when modeling contact behavior. Due to the absence of physical contact surface modeling, conventional contact algorithms may lead to an unrealistic contact area. To address this issue, many studies have adopted discrete orthogonal spring elements with a sufficiently high compressive stiffness along wall–foundation interfaces to provide an equivalent representation of contact behavior, corresponding to approach (c) described in Section 2.2.1.

Shell element-based models have been widely adopted for modeling both panelized CLT shear walls and PT CLT rocking walls. In modeling panelized CLT shear walls, contact effects are often incorporated either implicitly through the constitutive relationships of connection elements [36] or explicitly through distributed compression-only springs along the wall–lower floor interface [28]. The latter approach has been widely adopted and further refined in subsequent studies [17,18,31,35,38,62–64]. Two typical shell element-based models of panelized CLT walls are illustrated in Figure 6.



(**a**)

Figure 6. *Cont.*



(**b**)

Figure 6. Typical shell element-based models for panelized CLT shear wall: (**a**) implicit modeling approach [36]; (**b**) explicit modeling approach [28].

In PT CLT rocking wall models, the distributed-spring approach remains the primary strategy for representing the wall–lower floor interaction [13,23,56,59,60]. The key difference is the incorporation of PT tendon modeling, as detailed in Section 2.4.1. In addition, greater attention is given to the nonlinear response associated with local crushing at the wall–floor interface induced by rocking. Some studies assign nonlinear constitutive behavior to the entire wall panel [56], whereas others employ localized nonlinear regions only at locations susceptible to compression damage, such as wall corners and post-tensioning anchorage zones [23]. This localized nonlinear modeling strategy significantly reduces computational cost while maintaining the ability to capture the dominant crushing response.

3.2.2. Beam Element-Based Models

By modeling an entire wall segment with only a few elements, beam element-based models require far fewer degrees of freedom than shell element-based models and therefore are well suited for nonlinear dynamic time-history analyses of multi-story CLT structures. However, the reduction in element dimensionality also introduces several inherent limitations. First, beam element-based models are generally unable to explicitly model wall openings. As openings can substantially change the load transfer mechanism and stiffness distribution of CLT shear walls [19,68], the resulting changes in structural behavior are difficult to capture using one-dimensional beam elements. By contrast, shell element models can explicitly account for such geometric discontinuities. Second, beam element-based models are limited in representing local stress states because one-dimensional beam elements cannot explicitly capture multidimensional stress distributions, stress concentrations, or damage evolution in critical regions. Among these limitations, the inability to explicitly represent wall openings remains an inherent drawback of beam element-based approaches.

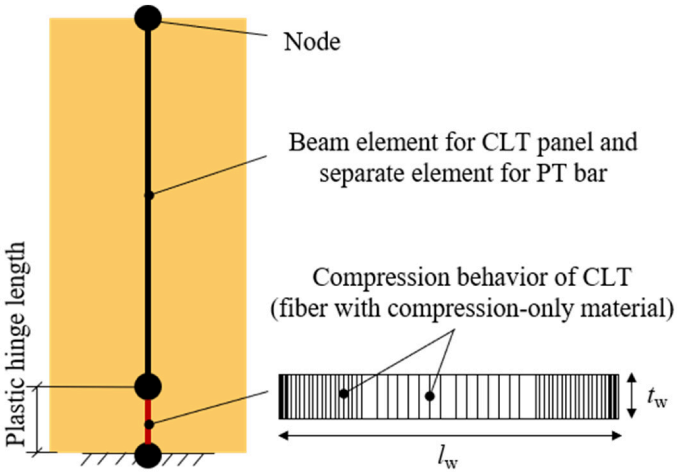
By comparison, considerable efforts have been made to address the second limitation through enhanced modeling of wall–lower floor contact behavior. As a result, fiber-based and multi-spring models have emerged, which implement the normal contact modeling approaches (b) and (c) described in Section 2.2.1, respectively.

1. Fiber-based models

In fiber-based beam models, CLT wall panels are modeled using beam–column elements with fiber sections. Under the plane-sections-remaining-plane assumption, the cross-section is discretized into multiple fibers, each of which can be assigned an independent constitutive relationship. By integrating the responses of individual fibers, the model can approximate sectional stress distributions and material nonlinearities within one-dimensional beam elements. For CLT walls, nonlinear fiber sections are typically assigned only within a predefined plastic hinge region near the wall base, while the remainder of the wall is elastic. Within the plastic hinge region, refined fiber discretization and nonlinear compressive constitutive models are commonly adopted near the wall edges to capture stress concentrations and localized crushing during rocking.

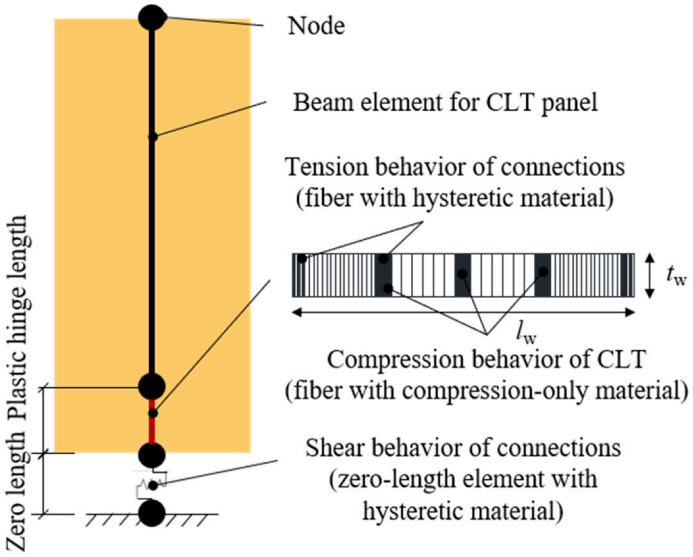
Several extensions of the fiber-based modeling framework have been developed for different CLT structural systems. As depicted in Figure 7a, Akbas et al. [24] modeled a PT rocking CLT wall panel using beam–column elements and introduced a predefined plastic hinge region with a length equal to twice the panel thickness. Within this region, fiber sections with compression-only constitutive models were used to capture localized wood crushing. A similar strategy was subsequently adopted by Zhu et al. [27]. Building upon this framework, Wang et al. [25] extended the model to panelized CLT shear walls by incorporating connection behavior into the fiber section, as shown in Figure 7b. The force–displacement relationships of connectors were converted into equivalent fiber-level stress–strain constitutive laws and assigned to fibers at the corresponding locations within the wall base plastic hinge region. The connector shear response was modeled separately using horizontal spring elements at the wall base.

Overall, fiber-based models efficiently capture localized nonlinear compression behavior within a simplified beam element framework, making them well suited for nonlinear analysis of CLT wall structures, with particular advantages for self-centering rocking walls.



(**a**)

Figure 7. *Cont.*



(**b**)

Figure 7. Typical fiber-based beam models: (**a**) fiber-based model for PT CLT shear wall [24]; (**b**) fiber-based model for panelized CLT shear wall [25].

2. Multi-spring models

Multi-spring models adopt a series of parallel nonlinear springs beneath the wall base to represent the wall–lower floor contact interface. These springs are employed to provide an equivalent representation of wall rocking behavior. Although this approach is conceptually similar to the multi-spring strategy adopted in shell element-based models (Section 3.2.1), the role and calibration of the springs differ substantially, as described in Section 2.2.1. In beam element-based models, the rocking behavior is simulated through the deformation of the multi-spring element. The plastic hinge length is therefore a critical modeling parameter, as it governs the conversion of stress–strain constitutive laws into equivalent force–displacement relationships. In most studies, the plastic hinge length is defined using principles similar to those adopted in fiber-based models.

The multi-spring concept was first proposed by Spieth [69] for the simulation of PT precast concrete shear walls. Sarti et al. [32] and Ganey [29] subsequently extended this approach to the numerical analysis of PT rocking walls. In their models, a series of parallel springs is connected to the base node of the wall beam element through rigid link elements to form a multi-spring foundation. The spring constitutive behavior is modeled with parameters calibrated against compression test data. As shown in Figure 8, Wichman et al. [57] adopted a similar modeling framework, with the spring properties derived directly from the compressive property of CLT. Building upon the two-dimensional model, Wichman et al. [57] and Berile [70] further extended the multi-spring approach to three-dimensional analysis, enabling the simultaneous representation of the in-plane and out-of-plane rocking behaviors of CLT shear walls.

It is worth noting that Wichman et al. [57,58] investigated the stiffness overlap issue inherent in multi-spring models and proposed a corresponding solution. In conventional implementations, the beam element and the wall base multi-spring element are connected in series, causing axial deformations to be represented by both components, thereby leading to an underestimation of the overall wall stiffness. To compensate for this effect, a geometric stiffness compensation approach was introduced in which a truss element is placed in parallel between the wall top node and the top node of the multi-spring element.

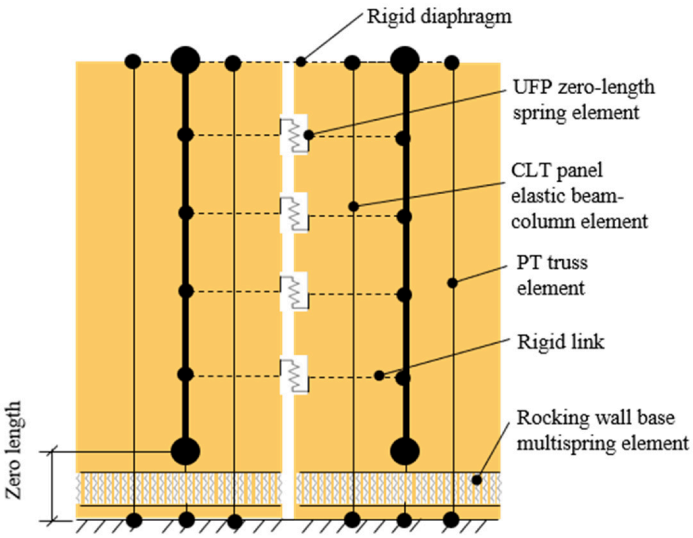


Figure 8. Typical multi-spring beam models [57].

3.3. Lumped-Spring Models (LSMs)

In large-scale nonlinear dynamic time-history analyses, researchers are generally more concerned about the global dynamic response of structures than the local stress states or detailed rocking mechanisms of individual wall panels. In this context, lumped-spring models (LSMs) have been widely adopted. These models simulate the overall nonlinear behavior of wall panels and connections through a small number of macro-spring elements representing key degrees of freedom. The global hysteretic responses of the structure can be reproduced with low computational cost. The spring properties are typically calibrated against full-scale wall tests or high-fidelity numerical simulations. As a result, the applicability of these models is generally restricted to structural configurations and boundary conditions that are consistent with those adopted in the calibration studies. Their simulation accuracy beyond the calibration range is often limited [71].

The selection of spring configurations primarily depends on the dominant deformation mechanism of the structural system. For panelized CLT shear walls, the seismic response is largely governed by the shear deformation of dowel-type connections. Consequently, translational spring and diagonal spring models are commonly adopted to simulate the global shear hysteretic behavior, as shown in Figures 9a and 9b, respectively. In translational spring models, the wall is typically represented by vertical elastic elements combined with horizontal nonlinear springs [31,38]. Alternatively, diagonal spring models employ rigid or elastic frame members together with nonlinear diagonal springs, transforming lateral deformation of the wall into the axial deformation of the springs [64]. In both approaches, spring constitutive relationships are generally calibrated from cyclic wall tests to reproduce strength degradation, stiffness degradation, and pinching effects.

For PT CLT rocking walls, rotational spring models are commonly employed because rocking is the dominant nonlinear deformation mechanism. Moment-rotation springs located at the wall base are used to capture the decompression, self-centering, and energy dissipation behavior of the system [23,32,72]. Figure 9c demonstrates a typical rotational spring model. Their constitutive relationships are generally established from analytical models and subsequently calibrated using numerical or experimental data.

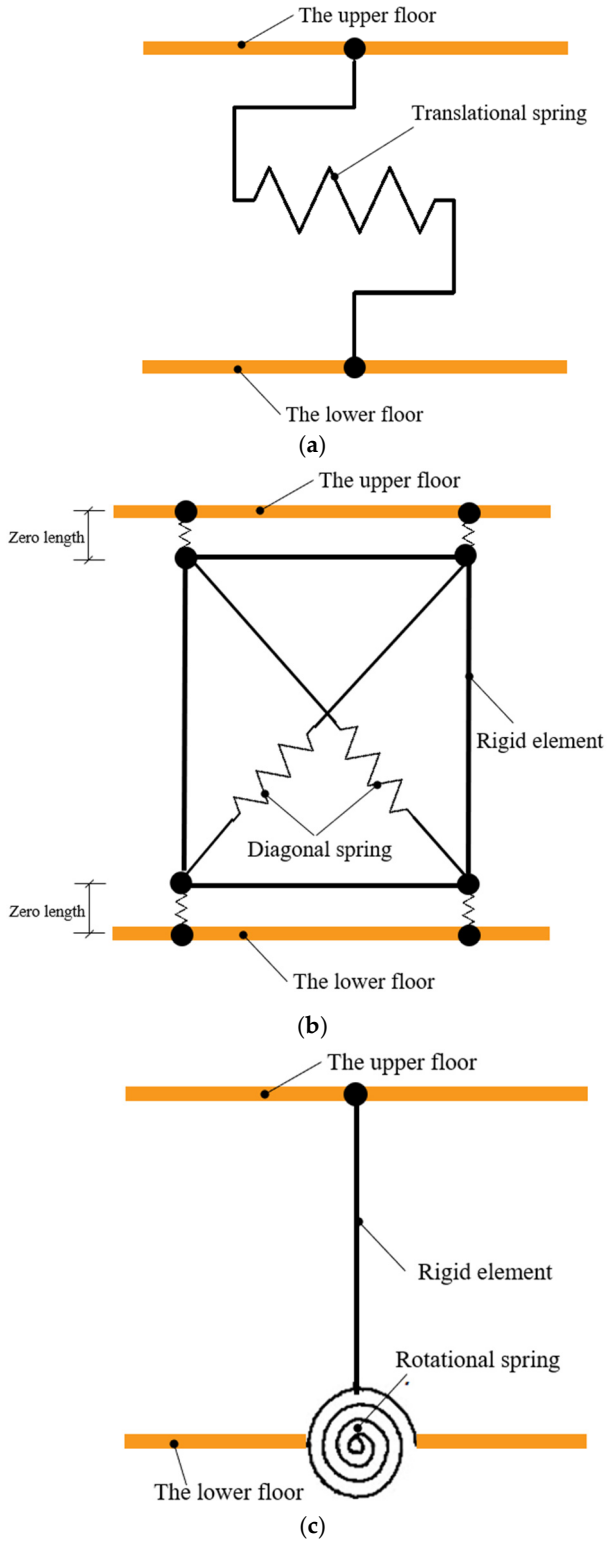


Figure 9. Typical lumped-spring models: (**a**) translational spring model; (**b**) diagonal spring model; (**c**) rotational spring model.

Despite their high computational efficiency, lumped-spring models rely on simplified representations of wall deformation mechanisms, which may limit their applicability to multi-story CLT structures [25]. Single-spring and diagonal spring models approximate wall behavior through equivalent shear deformation, whereas rotational spring models concentrate the nonlinear response into an equivalent wall base rotation. While these assumptions are often adequate for individual wall panels, they may become less accurate

in taller structures, where deformation patterns and stress distributions vary among stories, and the interaction between adjacent stories becomes difficult to capture, particularly the transfer of localized compressive forces from the upper story to the story below. As a result, modeling errors can accumulate with increasing structural height.

4. Applicability Assessment

The ranges of applicability of HFMs, CBMs, and LSMs are generally well defined because of their substantial differences in degrees of freedom, computational efficiency, and modeling accuracy [73]. However, systematic comparisons of alternative approaches within each category remain limited, causing confusion and difficulty in model selection. Since CBMs are the most widely adopted modeling category in both research and engineering practice, the shell element-based models, fiber-based beam models, and multi-spring beam models of the CBM category are selected for assessment and comparison. The three modeling approaches mainly differ in their treatment of normal contact behavior and their representation of CLT wall panels. Therefore, a basic panelized CLT shear wall is selected as the benchmark structure because its relatively simple and well-defined configuration allows these fundamental differences among the three CBMs to be examined while minimizing the influence of other modeling variables. A shell element-based model is first developed and validated against the experimental results reported by Hummel et al. [17]. Fiber-based and multi-spring models are then developed using the same geometric and construction details. The three models are compared in terms of structural response, deformation characteristics, and computational efficiency, providing a basis for selecting an appropriate CBM according to specific analysis objectives.

4.1. Model Description

The details of the benchmark CLT wall for the assessment and comparison can be found in the literature [17]. The descriptions of the modeling using shell element-based, fiber element-based, and multi-spring based approaches are provided below. The analysis platform OpenSeesPy 3.5.1.3 is adopted for the study [74].

4.1.1. Shell Element-Based Model

The shell element-based model is developed following the modeling strategy proposed by Hummel et al. [17], as illustrated in Figure 10. The CLT wall panel is represented by shell elements and assumed to behave as an isotropic linear elastic material with an elastic modulus of 6600 MPa and a Poisson's ratio of 0.3. Zero-length elements incorporating the SAWS constitutive model [75] are assigned to the locations of the hold-downs and angle brackets to represent connector behavior. The model parameters, calibrated from connection tests, are summarized in Table 3, where AB denotes the angle bracket, and HD denotes hold-down; the suffixes-S and -T indicate the shear and tension directions, respectively. Detailed definitions of all parameters can be found in Hummel et al. [17]. Along the wall–foundation interface, compression-only zero-length elements with the ENT material are introduced at all interface nodes to simulate normal contact behavior. The compressive stiffness of these elements is taken as 10^3 kN/mm.

A uniformly distributed vertical load of 10 kN/m is applied along the wall top. Owing to the single-story configuration and relatively low gravity load of the test specimen, friction at the wall–foundation interface is not considered in this study, as its estimated resistance is less than 7% of the measured lateral resistance. Cyclic lateral loading is imposed under displacement control through a prescribed horizontal displacement applied at the center node of the wall top. The shell mesh is discretized using a uniform element size of

250 mm × 250 mm, except for in the wall base boundary region. Figure 10 depicts the shell element-based model developed by Hummel [17].

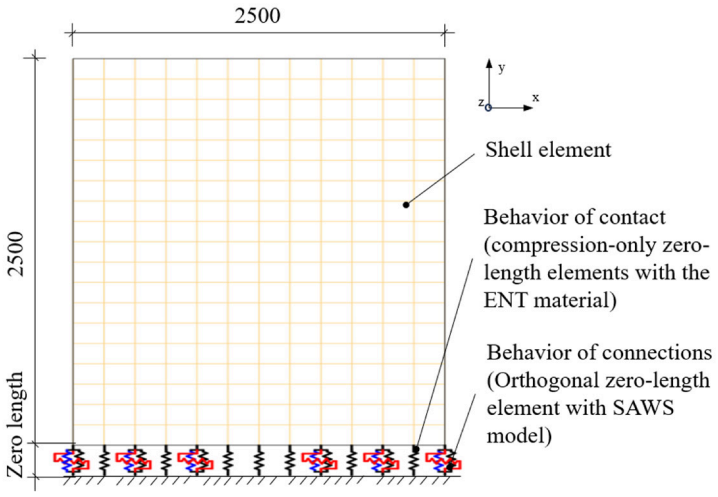


Figure 10. Shell element-based model proposed by Hummel et al. [17].

Table 3. SAWS parameters for connections [17].

Specimen	K_0 (kN/mm)	F_0 (kN)	F_1 (kN)	δ_u (mm)	r_1	r_2	r_3	r_4	α	β	K_y (kN/mm)	u_y (mm)	K_n (kN/mm)
AB-St-S	5.36	23.2	6.9	15.0	0.170	−0.17	3.0	0.04	0.25	1.05	-	-	-
HD-St-S	2.38	3.1	1.0	31.0	0.080	−0.17	3.0	0.02	0.60	1.10	-	-	-
AB-St-T	14.29	9.3	0.8	16.8	0.112	−0.10	3.0	0.025	0.45	1.05	2.50	−3.7	10^3
HD-St-T	9.64	21.4	1.2	26.0	0.180	−0.20	3.0	0.04	0.03	1.05	2.14	−4.0	10^3

4.1.2. Fiber-Based Model

The fiber-section-based model is developed following the modeling strategies proposed by Akbas et al. [24] and Wang et al. [25]. The wall geometry, loading protocol, material properties, and connection characteristics are kept consistent with those adopted in the shell element-based model. A schematic of the model is presented in Figure 11. The CLT wall panel is represented by beam–column elements and subdivided into an elastic region and a plastic hinge region located at the wall base. The plastic hinge length is taken as twice the CLT panel thickness. The wall segment outside the plastic hinge region is modeled using an elastic Timoshenko beam–column element, whereas the plastic hinge region is modeled using a displacement-based beam–column element with a fiber section.

Within the fiber section, fibers located at the geometric positions of the hold-downs and angle brackets are assigned constitutive relationships representing the tensile response of the corresponding connections (i.e., AB-St-T and HD-St-T in Table 3). The calibrated force–displacement relationships obtained from connection tests are converted into equivalent uniaxial stress–strain relationships at the fiber level. The fibers in the remaining wall base contact region are assigned a compression-only constitutive model (Concrete01) to represent localized CLT compression, with material parameters adopted from Wichman et al. [58]. To improve the representation of stress concentrations and localized crushing, a refined fiber discretization is employed near the wall edges. It should be noted that, according to the literature [25], the translational degree of freedom Uy and the rotational degree of freedom Rz at the wall base nodes are restrained. The shear–slip behavior of the connections is modeled separately using zero-length elements at the wall base, with the corresponding shear constitutive relationships (AB-St-S and HD-St-S in Table 3) assigned.

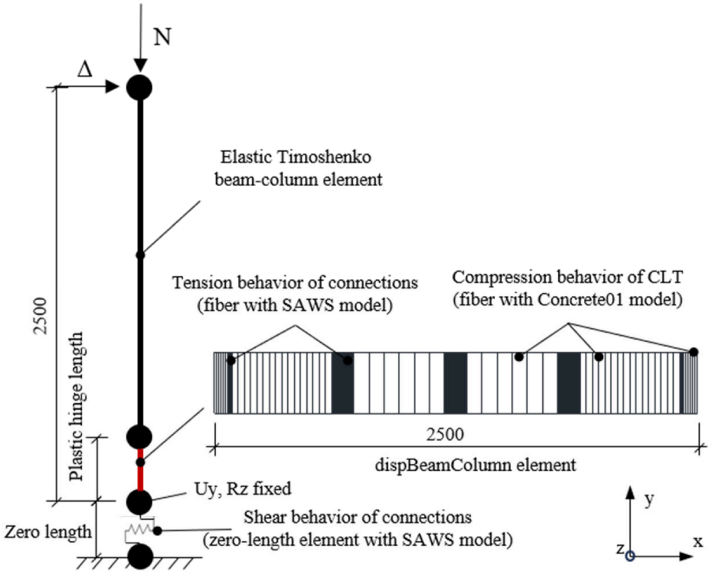


Figure 11. Fiber-based model (unit: mm).

4.1.3. Multi-Spring Model

Following the modeling concepts proposed by Demirci et al. [20], Sarti et al. [76], and Wichman et al. [57,58], a multi-spring model is developed for specimen W-CLT-St-10, as illustrated in Figure 12. The CLT wall panel is represented by an elastic Timoshenko beam element, while the wall–foundation interaction is modeled using a series of discrete zero-length springs distributed along the wall base. These springs are assigned a compression-only nonlinear constitutive model (Concrete01) to represent localized CLT compression and to reproduce the rocking behavior of the wall. The spring force–deformation relationships are derived from the CLT compressive stress–strain response using the same material properties adopted in the fiber-section-based model. The stiffness of each spring is determined according to its tributary area and the assumed plastic hinge length, as calculated using Equation (1). Additional nonlinear springs are introduced at the locations of the hold-downs and angle brackets to represent connector behavior. Their constitutive relationships are defined according to Table 3. Both the contact springs and connector springs are connected to the wall beam element through rigid links.

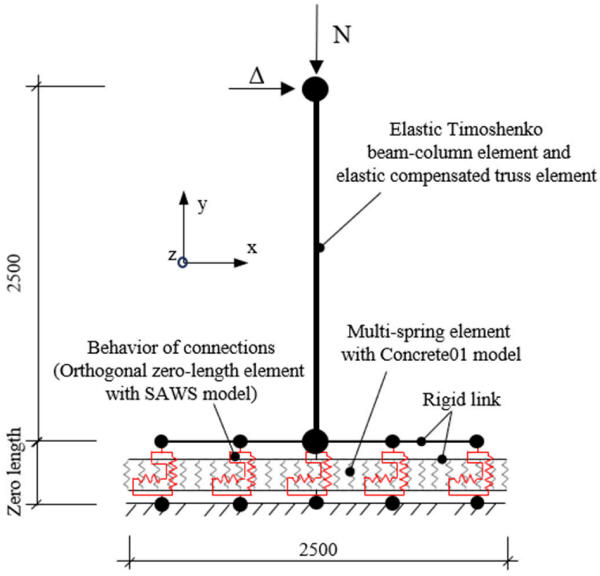


Figure 12. Multi-spring model (unit: mm).

To address the stiffness overlap issue inherent in multi-spring formulations, a truss element is placed in parallel with the wall beam element. The stiffness of the truss element is determined using the stiffness compensation approach proposed by Wichman et al. [58].

4.2. Comparison and Discussion

4.2.1. Model Validation

To validate the accuracy of the numerical modeling approach adopted in this section, the results obtained from the shell element-based model are first compared with the quasi-static experimental results and the finite element simulation results reported by Hummel et al. [17]. Figure 13 presents a comparison of the corresponding hysteretic responses. Table 4 summarizes the key response parameters obtained from the experimental and numerical results. F_{max} denotes the peak load, u_u denotes the ultimate displacement, u_y denotes the yield displacement, and k_{ini} denotes the initial stiffness. The values of u_y and k_{ini} are calculated based on the equivalent energy elastic–perfectly plastic (EEEP) curve [77]. Values in parentheses represent the relative errors with respect to the experimental results, calculated as (model − experiment)/experiment × 100%.

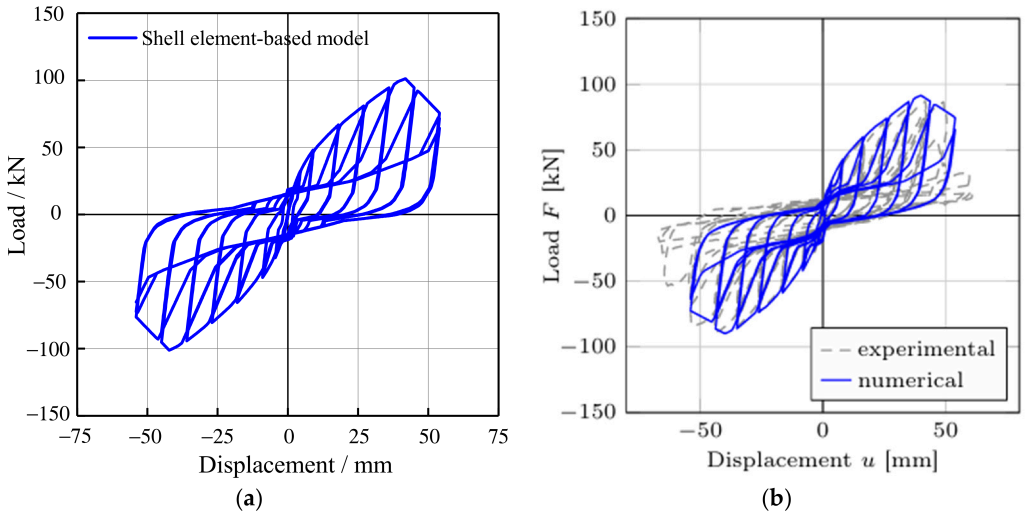


Figure 13. Comparison of hysteretic curves: (**a**) shell element-based model; (**b**) experimental and numerical results from Hummel et al. [17].

Table 4. Key response parameters: comparison of numerical and experimental results.

	F_{max} (kN)	u_u (mm)	u_y (mm)	k_{ini} (kN/mm)
Experimental results	88.2	55.5	13.3	5.6
Shell element-based model	101.1 (+14.6%)	51.7 (−6.9%)	13.9 (+4.5%)	5.9 (+5.4%)
Multi-spring model	100.8 (+14.3%)	54.3 (−2.2%)	15.6 (+17.3%)	5.2 (−7.1%)
Fiber-based model	101.2 (+14.7%)	50.8 (−8.5%)	14.7 (+10.5%)	5.6 (0%)

As shown in Figure 13, the shell element-based model developed in this study exhibits good agreement with both the experimental results and the numerical results reported in the literature in terms of the hysteretic response and key response parameters, with relative errors generally within approximately 10%. In particular, the model successfully reproduces the characteristic pinching behavior caused by dowel slip in the connections.

The close correlation between the numerical and experimental responses demonstrates that the adopted SAWS constitutive parameters and modeling strategy are capable of accurately representing the mechanical behavior of the CLT wall. Therefore, the proposed shell element-based model is considered sufficiently reliable and is subsequently used as the benchmark model for the comparative analyses presented in the following section.

4.2.2. Results Comparison and Discussion

1. Global hysteretic response

Further comparisons are conducted between the two beam element-based models (i.e., the fiber-based model and the multi-spring model) and the shell element-based model. As shown in Figure 14 and Table 4, the three models exhibit highly consistent global hysteretic responses and key response parameters. Notably, this agreement is achieved despite substantial differences in wall panel discretization, contact treatment, and connection implementation. The nonlinear constitutive laws assigned to the dowel-type connections constitute the only modeling strategy shared by all three models. The close agreement among the results therefore suggests that the global hysteretic response of the CLT shear wall is primarily governed by the nonlinear behavior of the connections. Specifically, the inelastic shear and uplift deformations of the wall base connections govern the energy dissipation, stiffness degradation, and strength evolution of the system. This finding confirms the connection-dominated feature of panelized CLT shear walls and explains why different modeling strategies can achieve similar global predictions when the connection response is accurately captured.

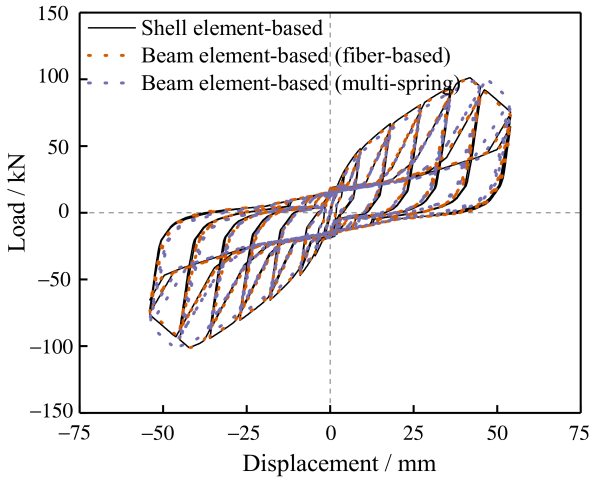


Figure 14. Comparison of hysteretic curves for the three models.

2. Deformation modes

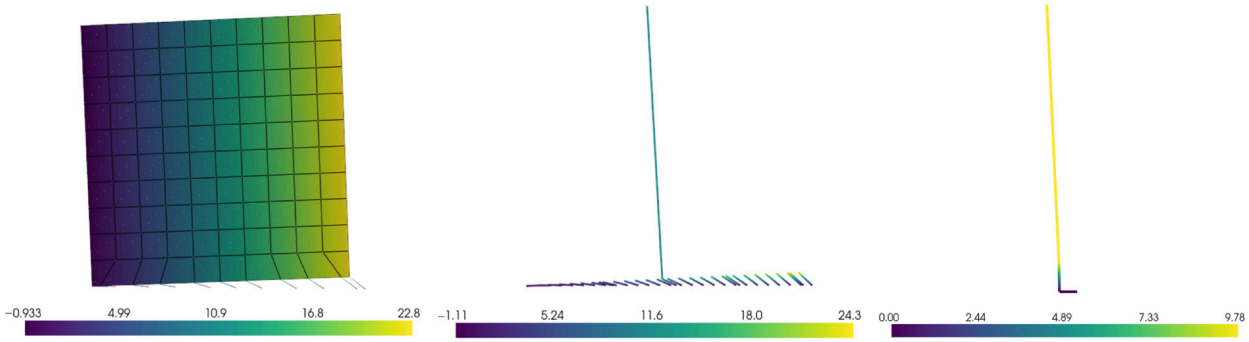
Although the three models produce highly consistent global hysteretic responses, their capabilities in representing the wall deformation mode differ significantly. Figure 15 presents the deformed configurations obtained from the three numerical models using the VFO visualization platform in OpenSeesPy, where the displacement scale represents the vertical displacement of the wall. The total deformation can be divided into three components: rocking, slip, and deformation of the CLT panel itself, which are calculated using Equations (2)–(4), respectively [17]. The average contributions over the selected displacement steps are presented in Table 4 as proportions of the top displacement u.

$$u_S = \frac{u_{l,x} + u_{r,x}}{2} \quad (2)$$

$$u_{\mathrm{R}} = \frac{(u_{\mathrm{l,y}} - u_{\mathrm{r,y}}) \cdot H_{\mathrm{w}}}{L_{\mathrm{w}}} \tag{3}$$

$$u_{\mathrm{CLT}} = u - u_{\mathrm{S}} - u_{\mathrm{R}} \tag{4}$$

where u_{S}, u_{R}, and u_{CLT} are the deformations due to slip, rocking, and deformation of the CLT panel itself, respectively; $u_{\mathrm{l,x}}$ and $u_{\mathrm{r,x}}$ are the displacements in the x direction of the leftmost and rightmost bottom corner nodes, respectively; $u_{\mathrm{l,y}}$ and $u_{\mathrm{r,y}}$ are the displacements in the y direction of the leftmost and rightmost bottom corner nodes, respectively; and H_{w} is the total height of the CLT wall.



(**a**) (**b**) (**c**)

Figure 15. Deformation modes in the final analysis step (amplification factor: 5): (**a**) shell element-based model; (**b**) multi-spring model; (**c**) fiber-based model.

The shell element-based model provides the most realistic representation of wall behavior. By employing two-dimensional shell elements, it can naturally capture both the rocking and sliding mechanisms of the CLT wall under lateral loading, resulting in deformation patterns that closely resemble those observed experimentally. Consistent with this behavior, the predicted deformation of the CLT panel differs from the experimental result by less than 10%, as summarized in Table 5. The multi-spring model also demonstrates a reasonable ability to reproduce the wall deformation mode. By introducing a series of discrete compression-only springs along the wall–foundation interface, the model represents wall rocking through spring deformation and can reproduce the migration of the compression zone along the wall base at the macroscopic level. The wall deformation calculated from the wall-side free nodes of the leftmost and rightmost contact springs is also in good agreement with the experimental result. In contrast, the fiber-based model provides the least realistic representation of the wall deformation. In this approach, the wall–foundation contact behavior and the responses of discrete connections are homogenized and incorporated into the fibers of a one-dimensional beam element. Consequently, the opening and closing of the wall–foundation interface cannot be explicitly represented, leading to noticeable discrepancies in the simulated deformation mode. The model fails to capture the rocking component and substantially overestimates the deformation of the CLT panel itself.

Table 5. Contributions to the overall deflection from rocking, slip, and CLT panel deformation: comparison of numerical and experimental results.

	u_{R}/u	u_{S}/u	u_{CLT}/u
Experimental results	64%	30%	6%
Shell element-based model	58%	38%	4%
Multi-spring model	58%	34%	8%
Fiber-based model	0	38%	62%

3. Computational efficiency and modeling recommendations

In terms of computational cost, substantial differences are observed among the three models under identical hardware conditions and convergence criteria. The fiber-based model completed the nonlinear analysis in only 1.0 s due to its limited number of degrees of freedom, demonstrating exceptional computational efficiency. The multi-spring model, despite incorporating rigid links and numerous nonlinear compression-only springs, required only 2.79 s and remained highly efficient. In contrast, the shell element-based model required 432.93 s, largely due to its dense two-dimensional mesh discretization and the associated increase in degrees of freedom.

Considering the comparative performance of the three models in terms of global response simulation, deformation representation, and computational efficiency, several recommendations can be made for the selection of component-based modeling approaches. The shell element-based model is most appropriate for detailed numerical investigations of individual wall panels or low-rise structures, particularly when local mechanical behaviors, such as in-plane stress distributions, localized crushing deformation, and complex contact interactions, are of primary interest. The multi-spring model achieves a balance between computational efficiency and the ability to capture wall base rocking behavior, making it well suited for seismic performance assessments and large-scale parametric studies of mid- and high-rise CLT shear wall structures. Although the fiber-based model substantially simplifies the wall–foundation interaction and therefore cannot accurately reproduce local deformation characteristics, it offers the highest computational efficiency among the three approaches. As a result, it is particularly suitable for nonlinear dynamic analyses of tall timber structures, as well as engineering applications that focus primarily on global response evaluation, such as inter-story drift, roof displacement, and overall lateral behavior.

5. Concluding Remarks and Future Research Needs

Recent code developments, including the introduction of Type IV-A construction in the 2021 IBC, together with the structural advantages of CLT, have stimulated growing interest in CLT shear wall structures. However, the codified CLT shear wall structure remains subject to height limitations, motivating the development of alternative systems, such as rocking, coupled, and pivoting CLT walls, which have been investigated primarily through experimental studies. Unlike steel and concrete structures, for which well-established constitutive models enable broadly applicable numerical simulations, the nonlinear response of CLT shear walls is largely governed by diverse and complex connections. Existing numerical models are often calibrated to individual experimental studies, while systematic comparisons and assessments of different modeling strategies remain limited. This paper presents a systematic review and comparative assessment of currently available numerical modeling strategies for CLT shear wall structures. The major conclusions and recommended directions for future research are summarized below.

5.1. Concluding Remarks

- Accurate simulation of CLT shear wall structures depends on the proper modeling of four key mechanisms: CLT panel behavior, contact behavior, nonlinear connection behavior, and self-centering behavior.
- Existing numerical models can be categorized into three types: HFMs, CBMs, and LSMs. The CBM is currently the most widely adopted framework and can be further divided into shell element-based, fiber-based, and multi-spring models.
- Comparative assessment within CBMs shows that, despite using different elements and distinct contact algorithms, all models can yield highly consistent global hysteretic

responses. This confirms that the lateral performance of panelized CLT shear walls is largely governed by connection behaviors.

- Considering the balance between modeling accuracy and computational efficiency, the comparative results provide preliminary guidance for model selection among CBMs. Shell element-based models are more suitable for refined analysis of individual wall piers or low-rise configurations where localized in-plane stress distributions and crushing behavior are of primary interest. Multi-spring macro-models provide a balance between computational efficiency and the representation of wall base rocking behavior, suggesting their potential for mid- to high-rise structural analyses and large-scale parametric studies. Fiber-based models offer the highest computational efficiency among the three approaches but have limited capability for capturing localized deformation modes due to their simplified representation of wall boundaries. Therefore, they may be advantageous for large-scale nonlinear dynamic analyses of tall timber structures, which focus primarily on global structural performance while requiring high computational efficiency.

5.2. Future Research Needs

- P–Δ (second-order) effects and their reasonable representation in numerical models of tall CLT shear wall structures require further investigation and experimental validation.
- Reliable macro-modeling approaches need to be developed for structural walls with special configurations, particularly walls with openings, where the representation of stiffness distribution and force transfer mechanisms remains challenging.
- Modeling techniques that can accurately capture three-dimensional interactions, including load transfer and deformation compatibility among walls, diaphragms, and adjacent structural components, need to be advanced.
- Generalizable numerical models with reduced reliance on test-specific calibration need to be developed. Given the diversity of CLT connector types and details, existing numerical models are often calibrated to individual experimental datasets, limiting their applicability beyond the tested systems. Future research should seek to develop physics-based modeling approaches that can predict connection and system behavior based on fundamental material and connection properties while using experimental data primarily for validation.

Author Contributions: Software, writing—original draft, and methodology, T.X.; conceptualization and resources, Y.W.; writing—review and editing, Y.W. and A.I. All authors have read and agreed to the published version of the manuscript.

Funding: This research received no external funding.

Data Availability Statement: The data and models that support the findings of this study are available from the corresponding author upon reasonable request.

Conflicts of Interest: The authors declare no conflicts of interest.

References

1. International Code Council. *International Building Code 2021*; International Code Council: Washington, DC, USA, 2021.
2. Breneman, S.; Podesto, L. Timber skyline: A review of structural systems for high-rise wood structures. In Proceedings of the SEAOC 2013 Convention, Structural Engineers Association of California, Sacramento, CA, USA, 18–21 September 2013.
3. Timmers, M.; Rogowksi, B.; Jacobs, A.; Jones, B. Mass timber high-rise design research: Museum tower in Los Angeles reimagined in mass timber. In Proceedings of the 2015 SEAOC Convention Proceedings, Seattle, WA, USA, 9–11 September 2015.
4. Reynolds, T.; Foster, R.; Bregulla, J.; Chang, W.S.; Harris, R.; Ramage, M. Lateral-load resistance of cross-laminated timber shear walls. *J. Struct. Eng.* **2017**, *143*, 06017006. [CrossRef]

5. American Society of Civil Engineers. *Minimum Design Loads and Associated Criteria for Buildings and Other Structures*; American Society of Civil Engineers: Reston, VA, USA, 2022.
6. Pei, S.; Fragiacomo, M.; Isoda, H.; Li, M.; Xiao, Y.; Smith, T. Codification and research for mass timber buildings in selected seismic regions: An overview. *Eng. Struct.* **2026**, *346*, 121685. [CrossRef]
7. Applied Technology Council. *Quantification of Building Seismic Performance Factors*; US Department of Homeland Security, FEMA: Washington, DC, USA, 2009.
8. Granello, G.; Palermo, A.; Pampanin, S.; Pei, S.; Van De Lindt, J. Pres-lam buildings: State-of-the-art. *J. Struct. Eng.* **2020**, *146*, 04020085. [CrossRef]
9. Chen, F.; Brown, J.R.; Li, Z.; Li, M. Numerical simulation and parametric analysis of posttensioned C-shaped CLT shear walls. *J. Struct. Eng.* **2025**, *151*, 04024198. [CrossRef]
10. Moerman, B.; Li, M.; Smith, T. Seismic design of hybrid coupled CLT shear walls with steel link beams. *Earthq. Eng. Struct. Dyn.* **2025**, *54*, 1520–1539. [CrossRef]
11. Araújo R., G.A.; Simpson, B.G.; Barbosa, A.R.; Pieroni, L.; Ho, T.X.; Orozco O., G.F.; Miyamoto, B.T.; Sinha, A. Experimental and numerical simulation of a three-story mass timber building with a pivoting wall and buckling-restrained boundary elements. *J. Struct. Eng.* **2025**, *151*, 04025089. [CrossRef]
12. Gavric, I.; Fragiacomo, M.; Ceccotti, A. Cyclic behavior of CLT wall systems: Experimental tests and analytical prediction models. *J. Struct. Eng.* **2015**, *141*, 04015034. [CrossRef]
13. Izzi, M.; Polastri, A.; Fragiacomo, M. Investigating the hysteretic behavior of cross-laminated timber wall systems due to connections. *J. Struct. Eng.* **2018**, *144*, 04018035. [CrossRef]
14. Foliente, G.C. Hysteresis modeling of wood joints and structural systems. *J. Struct. Eng.* **1995**, *121*, 1013–1022. [CrossRef]
15. D'Arenzo, G.; Casagrande, D.; Polastri, A.; Fossetti, M.; Fragiacomo, M.; Seim, W. CLT shear walls anchored with shear-tension angle brackets: Experimental tests and finite-element modeling. *J. Struct. Eng.* **2021**, *147*, 04021089. [CrossRef]
16. Rinaldi, V.; Casagrande, D.; Cimini, C.; Follesa, M.; Fragiacomo, M. An upgrade of existing practice-oriented FE design models for the seismic analysis of CLT buildings. *Soil Dyn. Earthq. Eng.* **2021**, *149*, 106802. [CrossRef]
17. Hummel, J. *Displacement-Based Seismic Design for Multi-Storey Cross Laminated Timber Buildings*; Kassel University Press GmbH: Kassel, Germany, 2017; Volume 8.
18. Hummel, J.; Seim, W. Displacement-based design approach to evaluate the behaviour factor for multi-storey CLT buildings. *Eng. Struct.* **2019**, *201*, 109711. [CrossRef]
19. Han, T.; Tesfamariam, S. Numerical analysis of CLT shear walls using high-fidelity model: Connection to building system. *J. Build. Eng.* **2023**, *72*, 106458. [CrossRef]
20. Demirci, C.; Malaga-Chuquitaype, C.; Macorini, L. Seismic shear and acceleration demands in multi-storey cross-laminated timber buildings. *Eng. Struct.* **2019**, *198*, 109467. [CrossRef]
21. Junda, E.; Malaga-Chuquitaype, C. Seismic acceleration demands in tall CLT buildings, predictive models and intensity measures. *Eng. Struct.* **2024**, *298*, 117024. [CrossRef]
22. Demirci, C.; Málaga-Chuquitaype, C.; Macorini, L. Seismic drift demands in multi-storey cross-laminated timber buildings. *Earthq. Eng. Struct. Dyn.* **2018**, *47*, 1014–1031. [CrossRef]
23. Wilson, A.W.; Motter, C.J.; Phillips, A.R.; Dolan, J.D. Modeling techniques for post-tensioned cross-laminated timber rocking walls. *Eng. Struct.* **2019**, *195*, 299–308. [CrossRef]
24. Akbas, T.; Sause, R.; Ricles, J.M.; Ganey, R.; Berman, J.; Loftus, S.; Dolan, J.D.; Pei, S.; van de Lindt, J.W.; Blomgren, H.E. Analytical and experimental lateral-load response of self-centering posttensioned CLT walls. *J. Struct. Eng.* **2017**, *143*, 04017019. [CrossRef]
25. Wang, X.; He, M.; Dong, H.; Li, Z. Numerical modeling strategies and parametric analyses of platform-type and balloon-type cross-laminated timber (CLT) shear walls under lateral loads. *Eng. Struct.* **2023**, *295*, 116857. [CrossRef]
26. Chen, Z.; Popovski, M. Material-based models for post-tensioned shear wall system with energy dissipators. *Eng. Struct.* **2020**, *213*, 110543. [CrossRef]
27. Zhu, H.; Bezabeh, M.A.; Iqbal, A.; Popovski, M.; Chen, Z. Seismic design and performance evaluation of post-tensioned CLT shear walls with coupling U-shaped flexural plates in Canada. *Earthq. Spectra* **2025**, *41*, 2203–2224. [CrossRef]
28. Hristovski, V.; Dujic, B.; Stojmanovska, M.; Mircevska, V. Full-scale shaking-table tests of XLam panel systems and numerical verification: Specimen 1. *J. Struct. Eng.* **2013**, *139*, 2010–2018. [CrossRef]
29. Ganey, R.S. Seismic Design and Testing of Rocking Cross Laminated Timber Walls. Master's Thesis, University of Washington, Seattle, WA, USA, 2015.
30. Kovacs, M.A.; Wiebe, L. Controlled rocking CLT walls for buildings in regions of moderate seismicity: Design procedure and numerical collapse assessment. *J. Earthq. Eng.* **2019**, *23*, 750–770. [CrossRef]
31. Sun, X.; He, M.; Li, Z.; Lam, F. Seismic performance assessment of conventional CLT shear wall structures and post-tensioned CLT shear wall structures. *Eng. Struct.* **2019**, *196*, 109285. [CrossRef]
32. Sarti, F. *Seismic Design of Low-Damage Post-Tensioned Timber Wall Systems*; University of Canterbury: Christchurch, New Zealand, 2015.

33. Rinaldin, G.; Amadio, C.; Fragiacomo, M. A component approach for the hysteretic behaviour of connections in cross-laminated wooden structures. *Earthq. Eng. Struct. Dyn.* **2013**, *42*, 2023–2042. [CrossRef]
34. Awad, V.; Giresini, L.; Koshihara, M.; Puppio, M.L.; Sassu, M. Experimental analyses and numerical models of CLT shear walls under cyclic loading. In *Wood in Civil Engineering*; InTech: Houston, TX, USA, 2017; p. 223.
35. Chen, J.; Wang, R.; Furuta, T.; Xiong, H. Experimental research on lateral performance of CLT shear walls with novel dissipative angle brackets and hold-downs. *J. Build. Eng.* **2024**, *86*, 108929. [CrossRef]
36. Rinaldin, G.; Fragiacomo, M. Non-linear simulation of shaking-table tests on 3-and 7-storey X-Lam timber buildings. *Eng. Struct.* **2016**, *113*, 133–148. [CrossRef]
37. Sustersic, I.; Fragiacomo, M.; Dujic, B. Seismic analysis of cross-laminated multistory timber buildings using code-prescribed methods: Influence of panel size, connection ductility, and schematization. *J. Struct. Eng.* **2016**, *142*, E4015012. [CrossRef]
38. Sun, X.; He, M.; Li, Z.; Shu, Z. Performance evaluation of multi-storey cross-laminated timber structures under different earthquake hazard levels. *J. Wood Sci.* **2018**, *64*, 23–39. [CrossRef]
39. Shahnewaz, M.; Tannert, T.; Alam, M.S.; Popovski, M. Capacity-based design for cross-laminated timber buildings. In Proceedings of the Structures Congress 2017, Denver, CO, USA, 6–8 April 2017; pp. 400–410.
40. Shahnewaz, M.; Pan, Y.; Shahria Alam, M.; Tannert, T. Seismic fragility estimates for cross-laminated timber platform building. *J. Struct. Eng.* **2020**, *146*, 04020256. [CrossRef]
41. Amini, M.O.; van de Lindt, J.W.; Rammer, D.; Pei, S. Rocking behavior of high-aspect-ratio cross-laminated timber shear walls: Experimental and numerical investigation. *J. Archit. Eng.* **2021**, *27*, 04021013. [CrossRef]
42. Dong, H.; He, M.; Wang, X.; Christopoulos, C.; Li, Z.; Shu, Z. Development of a uniaxial hysteretic model for dowel-type timber joints in OpenSees. *Constr. Build. Mater.* **2021**, *288*, 123112. [CrossRef]
43. Sandoli, A.; D'Ambra, C.; Ceraldi, C.; Calderoni, B.; Prota, A. Role of perpendicular to grain compression properties on the seismic behaviour of CLT walls. *J. Build. Eng.* **2021**, *34*, 101889. [CrossRef]
44. Pozza, L.; Saetta, A.; Savoia, M.; Talledo, D. Coupled axial-shear numerical model for CLT connections. *Constr. Build. Mater.* **2017**, *150*, 568–582. [CrossRef]
45. Shahnewaz, M.; Alam, S.; Tannert, T. In-plane strength and stiffness of cross-laminated timber shear walls. *Buildings* **2018**, *8*, 100. [CrossRef]
46. Gavric, I.; Fragiacomo, M.; Ceccotti, A. Cyclic behaviour of typical metal connectors for cross-laminated (CLT) structures. *Mater. Struct.* **2015**, *48*, 1841–1857. [CrossRef]
47. Scotta, R.; Marchi, L.; Trutalli, D.; Pozza, L. A dissipative connector for CLT buildings: Concept, design and testing. *Materials* **2016**, *9*, 139. [CrossRef] [PubMed]
48. Ganey, R.; Berman, J.; Akbas, T.; Loftus, S.; Daniel Dolan, J.; Sause, R.; Ricles, J.; Pei, S.; Lindt, J.V.D.; Blomgren, H.E. Experimental investigation of self-centering cross-laminated timber walls. *J. Struct. Eng.* **2017**, *143*, 04017135. [CrossRef]
49. Wang, X.; He, M.; Li, Z. Experimental testing of platform-type and balloon-type cross-laminated timber (CLT) shear walls with supplemental energy dissipators. *J. Build. Eng.* **2023**, *66*, 105943. [CrossRef]
50. Han, T.; Tobber, L.; Rodgers, G.; Tesfamariam, S. Hysteretic behavior of a cross-laminated timber building incorporating different energy dissipators. *Soil Dyn. Earthq. Eng.* **2025**, *188*, 109038. [CrossRef]
51. Sun, X.; He, M.; Li, Z.; Lam, F. Seismic performance of energy-dissipating post-tensioned CLT shear wall structures I: Shear wall modeling and design procedure. *Soil Dyn. Earthq. Eng.* **2020**, *131*, 106022. [CrossRef]
52. Han, T.; Popovski, M.; Tannert, T.; Tesfamariam, S. Numerical and analytical research of CLT shear wall structures considering the influence of orthogonal wall connections. *Structures* **2025**, *82*, 110623. [CrossRef]
53. Mallardi, M.G.; D'Arenzo, G.; Giordano, P.F.; Limongelli, M.P. Influence of perpendicular wall interactions on the lateral behaviour of multi-storey cross-laminated timber structures: An analytical and numerical study. *Eng. Struct.* **2025**, *340*, 120727. [CrossRef]
54. Ruggeri, E.; D'Arenzo, G.; Fossetti, M.; Seim, W. Investigating the effect of perpendicular walls on the lateral behaviour of Cross-Laminated Timber shear walls. *Structures* **2022**, *46*, 1679–1695. [CrossRef]
55. D'Arenzo, G.; Schwendner, S.; Seim, W. The effect of the floor-to-wall interaction on the rocking stiffness of segmented CLT shear-walls. *Eng. Struct.* **2021**, *249*, 113219. [CrossRef]
56. Sun, X.; He, M.; Li, Z. Experimental and analytical lateral performance of posttensioned CLT shear walls and conventional CLT shear walls. *J. Struct. Eng.* **2020**, *146*, 04020091. [CrossRef]
57. Wichman, S.; Berman, J.W.; Zimmerman, R.B.; Pei, S. Nonlinear Analysis of a 10-Story Building Shake Table Specimen with Mass Timber Rocking Walls. *J. Struct. Eng.* **2025**, *151*, 04025180. [CrossRef]
58. Wichman, S.; Berman, J.W.; Pei, S. Experimental investigation and numerical modeling of rocking cross laminated timber walls on a flexible foundation. *Earthq. Eng. Struct. Dyn.* **2022**, *51*, 1697–1717. [CrossRef]
59. Pozza, L.; Benedetti, L.; Tomei, V.; Ferracuti, B.; Zucconi, M.; Mazzotti, C. Cyclic response of CLT Post-Tensioned Walls: Experimental and numerical investigation. *Constr. Build. Mater.* **2021**, *308*, 125019. [CrossRef]

60. Tomei, V.; Zucconi, M.; Ferracuti, B. Post-tensioned rocking dissipative timber wall systems: Numerical prediction. *J. Build. Eng.* **2023**, *66*, 105897. [CrossRef]
61. Jerves, R.; Phillips, A.R. Cyclic testing and modeling of CLT rocking walls with modular base connections and LSL wall toes. *Eng. Struct.* **2024**, *321*, 118924. [CrossRef]
62. Bhandari, S.; Fischer, E.C.; Riggio, M.; Muszynski, L. Numerical assessment of In-plane behavior of multi-panel CLT shear walls for modular structures. *Eng. Struct.* **2023**, *295*, 116846. [CrossRef]
63. Javidi, S.; Gavric', I.; Fourlaris, G.; Salami, M.R. Seismic fragility analysis of a three-story cross-laminated timber building considering near and far field ground motions. *Bull. Earthq. Eng.* **2025**, *23*, 4047–4068. [CrossRef]
64. Sato, M.; Isoda, H.; Araki, Y.; Nakagawa, T.; Kawai, N.; Miyake, T. A seismic behavior and numerical model of narrow paneled cross-laminated timber building. *Eng. Struct.* **2019**, *179*, 9–22. [CrossRef]
65. Pozza, L.; Scotta, R.; Trutalli, D.; Polastri, A. Behaviour factor for innovative massive timber shear walls. *Bull. Earthq. Eng.* **2015**, *13*, 3449–3469. [CrossRef]
66. Zhu, H.; Bezabeh, M.A.; Iqbal, A.; Popovski, M.; Chen, Z. Determination of Canadian Seismic Force Modification Factors for Post-Tensioned Cross-Laminated Timber Rocking Walls. *J. Struct. Eng.* **2026**, *152*, 04025250. [CrossRef]
67. Salgado, R.A.; Guner, S. Characterization of the out-of-plane behavior of CLT panel connections. *Eng. Struct.* **2021**, *229*, 111596. [CrossRef]
68. Yasumura, M.; Kobayashi, K.; Okabe, M.; Miyake, T.; Matsumoto, K. Full-scale tests and numerical analysis of low-rise CLT structures under lateral loading. *J. Struct. Eng.* **2016**, *142*, E4015007. [CrossRef]
69. Spieth, H.A.; Carr, A.J.; Pampanin, S.; Murahidy, A.G.; Mander, J.B. *Modelling of Precast Prestressed Concrete Frame Structures with Rocking Beam-Column Connections*; University of Canterbury: Christchurch, New Zealand, 2004.
70. Berile, N.K.; Bezabeh, M.A. Performance-based wind design of tall mass timber buildings with coupled post-tensioned cross-laminated timber shear walls. *J. Wind Eng. Ind. Aerodyn.* **2025**, *257*, 105981. [CrossRef]
71. Chen, Z.; Tung, D.; Karacabeyli, E. Modelling Guide for Timber Structures. 2022. FPInnovations. Available online: https://web.fpinnovations.ca/modelling (accessed on 4 October 2026).
72. Wilson, A.W.; Motter, C.J.; Phillips, A.R.; Dolan, J.D. Seismic response of post-tensioned cross-laminated timber rocking wall buildings. *J. Struct. Eng.* **2020**, *146*, 04020123. [CrossRef]
73. Pozza, L.; Savoia, M.; Franco, L.; Saetta, A.; Talledo, D. Effect of different modelling approaches on the prediction of the seismic response of multi-storey CLT buildings. In *Timber Structures and Engineering*; WIT Press: Hampshire, UK, 2018; p. 163.
74. McKenna, F. OpenSees: A framework for earthquake engineering simulation. *Comput. Sci. Eng.* **2011**, *13*, 58–66. [CrossRef]
75. Folz, B.; Filiatrault, A. Cyclic analysis of wood shear walls. *J. Struct. Eng.* **2001**, *127*, 433–441. [CrossRef]
76. Pilon, D.S.; Palermo, A.; Sarti, F.; Salenikovich, A. Benefits of multiple rocking segments for CLT and LVL Pres-Lam wall systems. *Soil Dyn. Earthq. Eng.* **2019**, *117*, 234–244. [CrossRef]
77. *ASTM E2126-19*; Standard Test Methods for Cyclic (Reversed) Load Test for Shear Resistance of Vertical Elements of the Lateral Load Resisting Systems for Buildings. ASTM International: West Conshohocken, PA, USA, 2025.

Disclaimer/Publisher's Note: The statements, opinions and data contained in all publications are solely those of the individual author(s) and contributor(s) and not of MDPI and/or the editor(s). MDPI and/or the editor(s) disclaim responsibility for any injury to people or property resulting from any ideas, methods, instructions or products referred to in the content.